Consecutive-Contrastive Spherical U-net: Enhancing Reliability of Individualized Functional Brain Parcellation for Short-duration fMRI Scans

Dan Hu, Kangfu Han, Jiale Cheng, Gang Li✉
Department of Radiology and Biomedical Research Imaging Center, University of North Carolina at Chapel Hill, Chapel Hill, NC, 27599, USA
gang_li@med.unc.edu

Abstract. Individualized brain parcellations derived from functional MRI (fMRI) are essential for discerning unique functional patterns of individuals, facilitating personalized diagnoses and treatments. Unfortunately, as fMRI signals are inherently noisy, establishing reliable individualized parcellations typically necessitates long-duration fMRI scan (> 25 min), posing a major challenge and resulting in the exclusion of numerous short-duration fMRI scans from individualized studies. To address this issue, we develop a novel Consecutive-Contrastive Spherical U-net (CC-SUnet) to enable the prediction of reliable individualized brain parcellation using short-duration fMRI data, greatly expanding its practical applicability. Specifically, 1) the widely used functional diffusion map (DM), obtained from functional connectivity, is carefully selected as the predictive feature, for its advantage in tracing the transitions between regions while reducing noise. To ensure a robust depiction of brain network, we propose a dual-task model to predict DM and cortical parcellation simultaneously, fully utilizing their reciprocal relationship. 2) By constructing a stepwise dataset to capture the gradual changes of DM over increasing scan durations, a consecutive prediction framework is designed to realize the prediction from short-to-long gradually. 3) A stepwise-denoising-prediction module is further proposed. The noise representations are separated and replaced by the latent representations of a group-level diffusion map, realizing informative guidance and denoising concurrently. 4) Additionally, an N-pair contrastive loss is introduced to strengthen the discriminability of the individualized parcellations. Extensive experimental results demonstrated the superiority of our proposed CC-SUnet in enhancing the reliability of the individualized parcellation with short-duration fMRI data, thereby significantly boosting their utility in individualized studies.

Keywords: Individualized Brain Parcellation, Functional Diffusion Map (DM), Spherical U-net.

1 Introduction

Individualized functional brain mapping, derived from resting state functional MRI (rs-fMRI), is vital for detecting unique neural activity in individuals [1, 2], thereby enabling customized diagnostic and therapeutic strategies. Recent studies have demonstrated

how individualized parcellations can uncover variations in functional connectivity that correlate with cognitive traits [3] and identify robust biomarkers for neurological disorders [4-6], marking a significant shift towards individualized care [7,8]. However, fMRI signals, the foundational data for constructing functional connectome, inherently exhibit a low signal-to-noise ratio. To achieve reliable personalized brain functional mapping, significant research underscores the necessity for prolonged rs-fMRI sessions (>25 min) [9-11]. Adhering to this requirement poses significant difficulties in practical settings, especially for patients and young children [29]. For example, recent meta-analyses examining rs-fMRI data for depression [12] (23 studies) and schizophrenia [13] (36 studies) found an average scan duration of only 6 minutes. Consequently, numerous short-duration rs-fMRI datasets, whether previously collected or in progress, are unfortunately excluded from subject-level studies. To address this critical issue, existing studies have either proposed new measurements of functional connectivity [14, 15] or utilized bagging aggregation to augment the fMRI data [16], focusing on boosting reliability within the confines of short-duration scans themselves. However, they didn't tackle the most crucial question: how to ensure the individualized parcellations derived from short-duration scans sufficiently resemble those from their corresponding long-duration data, thus reaching the essence of increasing the reliability.

To bridge this gap, we develop a novel model, Consecutive-Contrastive Spherical U-net (CC-SUnet), to enhance the reliability of individualized brain parcellations by predicting long-duration data related parcellations based on short-duration rs-fMRI scans. Firstly, functional diffusion map (DM) [17, 18] is specially employed as the feature map of our prediction model, with its own prediction included as part of a dual task alongside individualized brain parcellation. By harnessing the DM's strength in capturing intrinsic networks and noise reduction, along with the dual task's ability to exploit its reciprocal relationship with brain parcellation, we effectively integrate critical information and mitigate noise, resulting in robust and reliable predictions. Then, to capture the gradual changes of DM over increasing scan durations, we construct a temporal stepwise dataset and design a consecutive prediction framework to realize the prediction from short-to-long gradually. Since the noise in short-duration fMRI data is not reasonably restrained due to insufficient scan time, a stepwise-denoising-prediction module is further proposed to dedicatedly handle the noise. In latent space, noise channels are separated and replaced by the representations of a group-level diffusion map, achieving informative guidance and denoising concurrently. Finally, an N-pair contrastive loss is introduced to maintain the variability in individuals and strengthen the discriminability of final parcellations. Experimental results showed that our proposed CC-SUnet not only enhances the test-retest reliability of parcellations obtained from short-duration fMRI scans but also significantly increases their similarity to those derived from long-duration data, greatly boosting the utility of short-duration fMRI scans.

2 Method

2.1 Model Description

The framework of our proposed model, Consecutive-Contrastive Spherical U-net (CC-

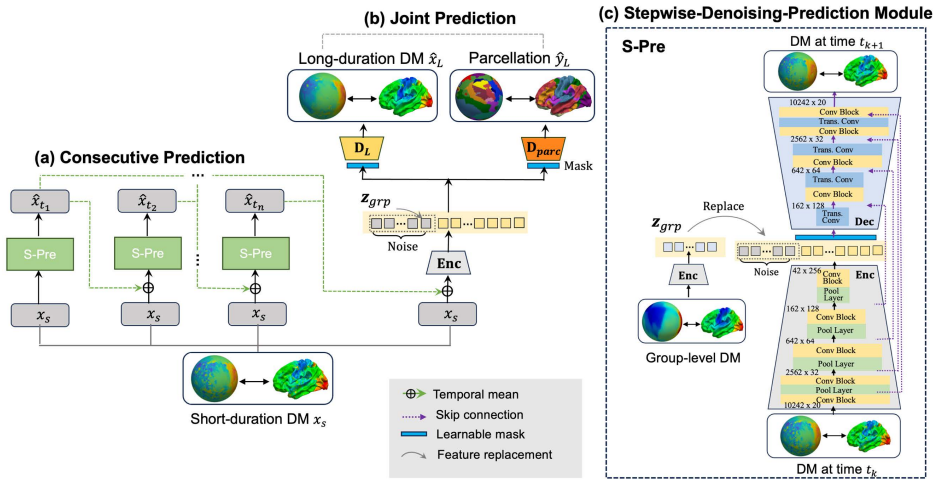

Fig. 1. The framework of our proposed CC-SUnet model.

SUnet), is depicted in **Fig. 1** and detailed below. It constitutes the stepwise diffusion map (DM) dataset construction, consecutive prediction, stepwise-denoising-prediction module (S-Pre), and joint prediction of DM and individualized parcellation.

Suppose we have a dataset of long-duration rs-fMRI scans and its corresponding individualized brain parcellations obtained from a given parcellation method [2], i.e., the paired samples $\{(\boldsymbol{B}_{iL}, y_i)|\boldsymbol{B}_{iL} \in X^{20,484\times T}, y_i \in Y^{20,484\times 1}, i = 1, \cdots, N\}$, N is the number of subjects, $\boldsymbol{B}_{iL}$ is the long-duration BOLD signals from subject i, 20,484 is the number of cortical vertices of the whole brain (10,242 per-hemisphere), T is the frames of the scan, y_i is the cortical parcellation map, and $Y = \{0, 1, 2, \cdots, 17\}$, since we discuss the popular 17-network functional parcellation [24] in this work. Notably, rather than embedding the process of the individualized parcellation for long-duration scans into our framework, we pre-calculate an individualized functional parcellation from a well-established method to serve as the ground truth. Our goal is to learn the mapping from short-duration DM to the brain parcellation derived from long-duration scans, regardless of the parcellation method used. This approach is flexible for any individualized brain parcellation method preferred by the users.

Stepwise diffusion map (DM) dataset construction. For a long-duration scan $\boldsymbol{B}_L$, a stepwise dataset is generated by setting a collection of time intervals $\{[t_0, s], [t_0, t_1], [t_0, t_2], \cdots, [t_0, t_n], [0, L]\}$, where $t_0 < s < t_1 < t_2 < \cdots < t_n < L$, as shown in **Fig. 2**. t_0 is a random start time to build up dataset, L is full scan time. $[t_0, s]$ is set to 5 minutes in this study, aligning with the minimal fMRI scan duration protocols used in most studies. This duration captures a relatively stable brain connectome, in contrast to the moment-to-moment fluctuations described by dynamic FC derived from fMRI scans lasting 30 to 60 seconds [28]. Each time interval relates to a fMRI signal clip and its corresponding functional connectivity (FC) is then computed by Pearson's correlation between vertices followed by Fisher z-transformation, leading to a stepwise FC dataset $\{\boldsymbol{F}_s, \boldsymbol{F}_{t_1}, \cdots, \boldsymbol{F}_{t_n}, \boldsymbol{F}_L\}$. Then, to align subjects, a group-level FC matrix $\boldsymbol{F}_{grp}$ and a joint

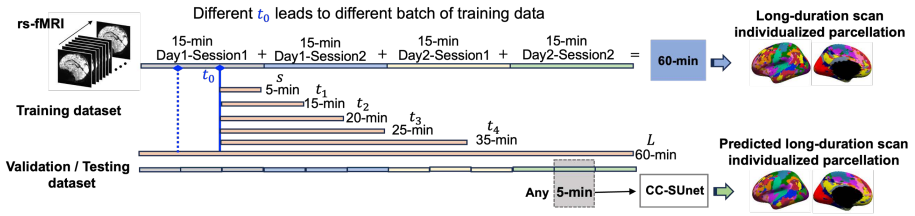

Fig. 2. The construction of training/validation/testing dataset, taking HCP dataset as an example.

embedding strategy [19, 30] are introduced for DM computation. For an $\boldsymbol{F}_t$, $t \in \{s, t_1, \cdots, t_n, L\}$, a joint similarity matrix $\boldsymbol{W}_t$ is computed by concatenating FCs as

$$\boldsymbol{W}_t = [\boldsymbol{F}_t, \boldsymbol{F}_{t,grp}; \boldsymbol{F}_{t,grp}^T, \boldsymbol{F}_{grp}] \tag{1}$$

where $\boldsymbol{F}_{t,grp}$ is the correlation between $\boldsymbol{F}_{grp}$ and $\boldsymbol{F}_t$ based on Pearson's correlation. Then, the diffusion embedding algorithm [17] is applied on $\boldsymbol{W}_t$, resulting in a set of components as $\{[\boldsymbol{x}_t, \boldsymbol{x}_{grp}] | \boldsymbol{x}_t, \boldsymbol{x}_{grp} \in \mathbb{R}^{20,484 \times M}\}$. $\boldsymbol{x}_t$ and $\boldsymbol{x}_{grp}$ lie in a common coordinate space. M is the reduced dimension in DM space and determined by the accumulated contribution of the eigenvectors. M is set as 20 in our study. The final alignment of $\boldsymbol{x}_t$ across individuals is determined by a Procrustes transformation between $\boldsymbol{x}_{grp}$ and the group-level DM $\bar{\boldsymbol{x}}_{grp}$ obtained by $\boldsymbol{F}_{grp}$.

Consecutive prediction. Instead of predicting the DMs of long-duration scan from the brief fMRI data within one step, a consecutive prediction model is designed to realize a prediction chain as $\boldsymbol{x}_s \to \boldsymbol{x}_{t_1} \to \cdots \to \boldsymbol{x}_{t_n}$. n is set as 3 in our study for simplicity. This consecutive architecture not only captures the gradual changes of DM along with the increase of scan duration, but also minimizes the uncertainty in long range prediction. As shown in **Fig. 3**, each prediction step is implemented by an S-Pre module (detailed in the following section) and serves as a checkpoint to reassess conditions and adjust the subsequent learning. The function of S-Pre module is to predict DM $\boldsymbol{x}_{t_{k+1}}$ by the average of precedent DMs $\{\boldsymbol{x}_s, \hat{\boldsymbol{x}}_{t_1}, \cdots, \hat{\boldsymbol{x}}_{t_{k-1}}, \hat{\boldsymbol{x}}_{t_k}\}$, denoted as $\bar{\bar{\boldsymbol{x}}}_{t_k}$, i.e.,

$$\hat{\boldsymbol{x}}_{t_{k+1}} = \text{S-Pre}(\bar{\bar{\boldsymbol{x}}}_{t_k}),\ \bar{\bar{\boldsymbol{x}}}_{t_k} = \frac{1}{k+1}(\boldsymbol{x}_s + \textstyle\sum_{t=t_1,\cdots,t_k} \hat{\boldsymbol{x}}_t) \tag{2}$$

The previously predicted DM and $\boldsymbol{x}_s$ are specifically included into the S-Pre to avoid forgetting individualized characteristics because of long distance mapping.

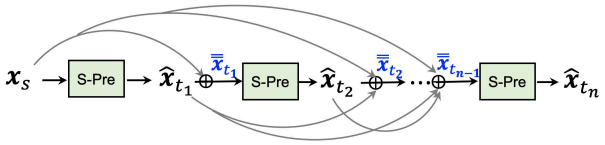

Fig. 3. The consecutive prediction based on stepwise-denoising-prediction modules.

Stepwise-denoising-prediction module (S-Pre). The backbone of S-Pre is a spherical U-net, which shares the same architecture with U-net in Euclidean space while only

replacing all operations with their spherical operation counterparts based on the 1-ring filter on icosahedron discretized spheres [20, 21]. Its advantage in extracting contextual and localization information on cortical surface makes it a perfect fit for parcellation studies. As shown in **Fig. 1(c)**, it has an encoder path and a decoder path, each with five resolution steps (10,242, 2,562, 642, 162, 42). The shared encoder (**Enc**) is composed of 5 spherical convolution blocks and 4 spherical pooling layers. Each convolution block is constituted of one 1-ring convolution layer, one group normalization layer and one linear layer with LeakyReLU as its activation function. Then the shared decoder (**Dec**) is composed of repetitive spherical convolutions and transposed convolutions and to generate the outputs from the feature maps generated in the encoder.

Compared with long-duration scans, the main issue of short-duration scans is the inherent noise, which is not reasonably restrained by enough scan time. To address this challenge, we propose to separate the noise in the latent space and replace it with group-level DM latent representation as guidance. Specifically, in S-Pre, the encoded representation of $\overline{\overline{\boldsymbol{x}}}_{t_k}$, $\boldsymbol{z}_{t_k}$, is first separated into two parts: $noise(\boldsymbol{z}_{t_k})$ and $info(\boldsymbol{z}_{t_k})$. Then, $noise(\boldsymbol{z}_{t_k})$ is discarded and replaced by $\boldsymbol{z}_{grp} = conv(\mathbf{Enc}(\boldsymbol{x}_{grp}))$. Of note, instead of directly concatenating $\boldsymbol{z}_{grp}$ to $\boldsymbol{z}_{t_k}$, a part of $\boldsymbol{z}_{t_k}$ is separated and removed as $noise(\boldsymbol{z}_{t_k})$, aiming to eliminating mixed noise information in $\boldsymbol{z}_{t_k}$. $conv(\cdot)$ is a convolution layer to adjust the channel number of $\mathbf{Enc}(\boldsymbol{x}_{grp})$ to match with the noise. We set the dimension of $\boldsymbol{z}_{t_k}$, $noise(\boldsymbol{z}_{t_k})$, $info(\boldsymbol{z}_{t_k})$, and $conv(\mathbf{Enc}(\boldsymbol{x}_{grp}))$ as 42x256, 42x64, 42x192, and 42x64 in our study. Furthermore, the concatenation of $info(\boldsymbol{z}_{t_k})$, and $conv(\mathbf{Enc}(\boldsymbol{x}_{grp}))$ passes through a learnable mask layer with W as its weights, allowing the decoder **Dec** to focus on the most relevant information thus enforcing the effect of denoising. The main idea of S-Pre is described as follows,

$$\hat{\boldsymbol{x}}_{t_{k+1}} = \mathbf{Dec}\left(W \cdot \left[info\left(\mathbf{Enc}(\overline{\overline{\boldsymbol{x}}}_{t_k})\right), conv\left(\mathbf{Enc}(\boldsymbol{x}_{grp})\right)\right]\right) \tag{3}$$

Joint prediction of DM and individualized parcellation. To avoid intermediate parcellations obtained from noisy DM interfere the denoising process, the task of the individualized parcellation is only included into the dual-task module until the DM of the last intermediate timepoint t_n is predicted. The input of the dual task module is $\overline{\overline{\boldsymbol{x}}}_{t_n}$, which is the average of $\{\boldsymbol{x}_s, \hat{\boldsymbol{x}}_{t_1}, \cdots, \hat{\boldsymbol{x}}_{t_{n-1}}, \hat{\boldsymbol{x}}_{t_n}\}$. As shown in **Fig. 1(b)**, after encoded with the shared encoder **Enc** and a denoising layer, the embedded features are fed into two branches, long-duration DM prediction and individualized parcellation, separately. The two branches are composed of a learnable mask layer (W_L/W_{parc}) and a decoder ($\mathbf{D_L}$ /$\mathbf{D_{parc}}$), sharing the same framework of the ones described in S-Pre. Thus, the final prediction $\hat{\boldsymbol{x}}_L$ and $\hat{y}$ are obtained and shown as follows:

$$\hat{\boldsymbol{x}}_L = \mathbf{D_L}(W_L \cdot \boldsymbol{z}_{t_n}), \hat{y} = \mathbf{D_{parc}}(W_{parc} \cdot \boldsymbol{z}_{t_n}) \tag{4}$$

$$\boldsymbol{z}_{t_n} \triangleq \left[info\left(\mathbf{Enc}(\overline{\overline{\boldsymbol{x}}}_{t_n})\right), conv\left(\mathbf{Enc}(\boldsymbol{x}_{grp})\right)\right] \tag{5}$$

Prediction loss. The predicted DM is evaluated with Pearson's correlation coefficient (PCC) and mean squared error (MSE), while the difference between the predicted and expected individualized parcellation is measured by weighted cross entropy loss.

Specifically, DM prediction loss is defined as

$$\mathcal{L}_{DM}^{PCC} = \frac{1}{n+1}\sum_{\boldsymbol{x_t}=\boldsymbol{x_{t_1}},\cdots,\boldsymbol{x_{t_n}},\boldsymbol{x_L}} \mathbb{E}_v(1 - corr(\boldsymbol{x}_t, \widehat{\boldsymbol{x}}_t)) \tag{6}$$

$$\mathcal{L}_{DM}^{MSE} = \frac{1}{n+1}\sum_{\boldsymbol{x_t}=\boldsymbol{x_{t_1}},\cdots,\boldsymbol{x_{t_n}},\boldsymbol{x_L}} \mathbb{E}_v(\|\boldsymbol{x}_t - \widehat{\boldsymbol{x}}_t\|_2^2) \tag{7}$$

$$\mathcal{L}_{DM} = \lambda\mathcal{L}_{DM}^{MSE} + \mathcal{L}_{DM}^{PCC},\ \lambda \text{ is a trade-off parameter} \tag{8}$$

The weighted cross entropy loss is defined as

$$\mathcal{L}_{parc} = -\mathbb{E}_v(w_c \log\left(\frac{\exp(P(c|v))}{\sum_{j=1}^{C}\exp(P(j|v))}\right)) \tag{9}$$

where v is a vertex on the surface, c is the parcellation label, C is the total network number in y and equals to 17 in our study, $P(j|v)$ is the probability of v being predicted as network j, w_c is the inverse of the area of c^{th} network in y, $\mathbb{E}$ is the expectation across the whole cortical surface.

N-pair contrastive loss. In individualized parcellation, test-retest similarity and inter-subject variability hold equal importance. The former ensures reliability, while the latter guarantees distinguishability. During learning, a mini-batch N-pair loss [25] is introduced to boost test-retest similarity and inter-subject variability simultaneously. For the short-duration DM $\boldsymbol{x}_s^i$ of subject i, taken as the anchor and obtained from the fMRI signal clip from the time interval $[t_0, s]$, its positive example is designed as $\{\boldsymbol{x}_{s\Delta}^i\}$, where $\boldsymbol{x}_{s\Delta}^i$ is the DM of time intervals $[t_0 + \Delta, s + \Delta]$. Δ is set as 15 minutes in our study. $\boldsymbol{x}_s^i$ and $\boldsymbol{x}_{s\Delta}^i$ will be enforced to be similar in the embedding space and lead to the same prediction since they are from the same subject. The negative examples of $\boldsymbol{x}_s^i$ are defined as $\{\boldsymbol{x}_s^j | j \neq i\}$. Thus, the N-pair contrastive loss is defined as

$$\mathcal{L}_{contra} = -\sum_{i=1}^{K}\sum_{j=1}^{K}\left(w_{ij}\log\left(\frac{\exp(\text{logit}_{ij})}{\sum_{k=1}^{K}\exp(\text{logit}_{ik})}\right)\right) \tag{10}$$

$$\text{logit}_{ii} = \left(\frac{\boldsymbol{z}_s^i}{\|\boldsymbol{z}_s^i\|_2}\right)\cdot\left(\frac{\boldsymbol{z}_{s1}^i}{\|\boldsymbol{z}_{s\Delta}^i\|_2}\right),\ \text{logit}_{ij,j\neq i} = \left(\frac{\boldsymbol{z}_s^i}{\|\boldsymbol{z}_s^i\|_2}\right)\cdot\left(\frac{\boldsymbol{z}_s^j}{\|\boldsymbol{z}_s^j\|_2}\right)$$

where $\boldsymbol{z}_s^i$, $\boldsymbol{z}_{s\Delta}^i$ and $\boldsymbol{z}_s^j$ are corresponding embedding of $\boldsymbol{x}_s^i$, $\boldsymbol{x}_{s\Delta}^i$ and $\boldsymbol{x}_s^j$ in the dual-task module, K is the batch size, and w_{ij} equals to 0 when $j \neq i$ or 1 otherwise.

Full objective. Combining DM prediction loss, parcellation loss, and contrastive loss, the full loss is written as:

$$\mathcal{L}_{DM} = \beta\mathcal{L}_{DM} + \gamma\mathcal{L}_{parc} + \mathcal{L}_{contra} \tag{11}$$

where β and γ are trade-off parameters.

2.2 Model Evaluation

For the given dataset $\{(\boldsymbol{x}_{iL}, y_i) | i = 1, \cdots, N\}$, the predicted DM is evaluated by Pearson's correlation coefficient (**PCC**) and mean absolute error (**MSE**). The predicted individualized parcellation is evaluated by following measures: 1) **validity** of the parcellation: measured by the dice similarity coefficient (**DSC**) between the expected brain parcellation y_i obtained by long-duration rs-fMRI scan and the predicted parcellation $\hat{y}_i$ from the short-duration scan,

$$\text{Validity}=\frac{1}{N}\sum_{i=1}^{N}\text{DSC}(y_i,\hat{y}_i)=\frac{1}{N}\sum_{i=1}^{N}\left(\frac{1}{17}\sum_{c=1}^{17}\frac{2\cdot|y_i(c)\cap\hat{y}_i(c)|}{|y_i(c)|+|\hat{y}_i(c)|}\right) \quad (12)$$

2) **Test-retest reliability:** measured by the DSC between the predicted parcellation $\hat{y}_i$ and $\hat{y}_{i\Delta}$ obtained from the positive pair $\boldsymbol{x}_s^i$ and $\boldsymbol{x}_{s\Delta}^i$, respectively. 3) **Inter-subject variability**: measured by the DSC between the predicted parcellation $\hat{y}_i$ and $\hat{y}_j$ $(j \neq i)$. The effect size of the variability is measured by **Cohen's d** [26]. 4) **Homogeneity (Homo)**: measured by the consistency of the functional connectivity patterns within each network, i.e., averaged Pearson's correlations of fMRI signals between all pairs of vertices within each network, adjusted for the network size.

3 Experiments

3.1 Data Description

The experimental data was from the HCP S900 data release [22]. 350 subjects (180 female, age range 22–35 years) were used in this study. 200, 50, and 100 subjects are partitioned as training, validation, and testing dataset. Group-level DM was computed from the training set. Each participant underwent two fMRI sessions on two different days and acquired 60-minute rs-fMRI in total. The "ICA-FIX" denoised fMRI data were preprocessed in the HCP pipeline using FSL, FreeSurfer, and Connectome Workbench's functions [27]. Each subject's preprocessed rs-fMRI data were resampled to a standard cortical surface (fsaverage5) with 10,242 vertices on each hemisphere. The long-duration parcellation was obtained by using an iterative algorithm [2]. The model, once trained on the HCP dataset, was further evaluated using the Midnight Club dataset (MSC) [23] to assess its applicability of enforcing the reliability of individualized parcellation with short-duration scan on an independent dataset. There are 10 subjects in the MSC dataset, and each has 5 hours of rs-fMRI scan. During testing, the rs-fMRI scan of each subject was segmented into extremely short non-overlapping 2-min data and the expected parcellation and DM were generated with the corresponding full scan.

3.2 Validation of CC-SUnet

We compared the proposed CC-SUnet model with the following six methods including four well recognized methods: (1) the original results obtained from short-duration scan (None) using the original method in [2]; (2) U-net (U-net), sharing the same settings as CC-SUnet, while only changing operations on icosahedron discretized spheres to Euclidean space; (3) Autoencoder with convolution operation (AE-CNN), sharing the same settings as U-net but removing the skip connection; (4) Multilayer Perceptron network (MLP); Two models derived from our CC-SUnet for validating our proposed strategies, including: (5) without contrastive loss (CC-SUnet_w/o C); (6) without consecutive prediction framework (CC-SUnet_direct).

All models were implemented with PyTorch and optimized with Adam algorithm alongside a strategy of reducing the learning rate once validity dice stagnates for 2 epochs. The initial learning rate was 0.001, the batch size was set as 5, $\lambda = \beta = 1$, and $\gamma = 1.1$. The comparison results are reported in **Table 1** and visualized in **Fig. 4**. Our

CC-SUnet model outperformed other competing methods by increasing the reliability of the parcellation from 0.543 to 0.845 and the validity from 0.619 to 0.772. When removing the contrastive loss or the consecutive prediction architecture, the accuracy of the model was reduced, further validating the effectiveness of the proposed strategies. Notably, the low variability (0.375) of the original method (None) is mainly due to noise dominance, while AE-CNN's high reliability (0.938) is attributed to its consistent parcellations, see **Fig. 4**. We further tested the utility of the trained model on the MSC dataset. As depicted in **Table 2**, even with all the parameters frozen, the reliability of the individualized parcellation was improved from 0.592 to 0.800, while increasing the validity, Cohen's d, and homogeneity of the parcellation concurrently. Of note, with the original method (None), the homogeneity of individualized parcellation obtained from the MSC data is 0.269. This value is higher than that obtained from the HCP data, likely due to site effects, and does not hold significant meaning in our comparison.

Table 1. The comparison of CC-SUnet with six competing methods on HCP dataset. (Short duration scans of 5-minute data. Mean values are reported, ↓ means the lower value is better)

	DM Prediction		**Individualized Parcellation Prediction**				
	PCC	MSE↓	Validity	Reliability	Variability↓	Cohen's d	Homo
None	0.684	0.071	0.619	0.543	0.375	0.682	0.115
U-net	0.815	0.034	0.735	0.824	0.712	0.577	0.122
AE-CNN	0.716	0.049	0.678	0.938	0.925	0.015	0.106
MLP	0.752	0.038	0.553	0.508	0.354	0.578	0.101
C-SUnet_w/o C	0.855	0.028	0.770	0.843	0.709	0.752	0.125
CC-SUnet_direct	0.797	0.036	0.761	0.828	0.698	0.720	0.123
Our CC-SUnet	0.865	0.026	0.772	0.845	0.681	0.795	0.131

Table 2. The validation of trained CC-SUnet on the independent MSC dataset (extremely short duration scans of only 2-minute data).

	DM Prediction		**Individualized Parcellation Prediction**				
	PCC	MSE↓	Validity	Reliability	Variability↓	Cohen's d	Homo
None	0.765	0.056	0.653	0.592	0.455	0.615	0.269
CC-SUnet	0.792	0.048	0.760	0.800	0.676	0.652	0.295

4 Conclusion

In this study, we proposed the Consecutive-Contrastive Spherical U-net (CC-SUnet), a novel framework designed unprecedentedly to realize the prediction of long-duration scan derived individualized brain parcellation using short-duration fMRI scans. Experimental results demonstrate CC-SUnet's remarkable effectiveness in improving the validity, reliability, and variability, significantly advancing the application of short

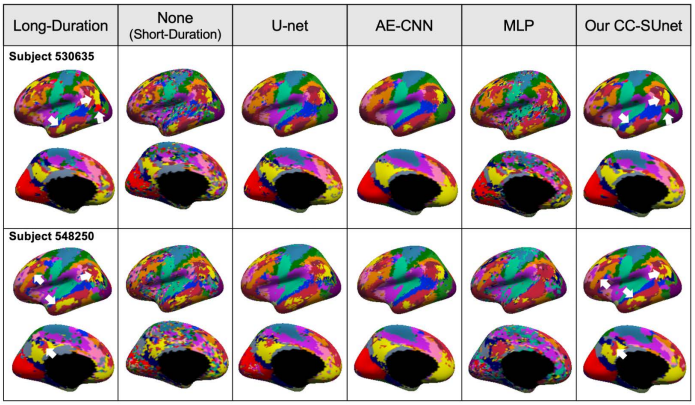

Fig. 4. The visual comparison of the predicted individualized brain parcellation of two random subjects in HCP**.** Our proposed CC-SUnet significantly increased the marginal sharpness, the within-network consistency, and the similarity with the parcellations derived by long-duration scans, while maintained the personalized characteristics as indicating by white arrows.

duration fMRI in individualized studies. This model greatly facilitates the broader use of existing large amount of low-quality fMRI for research at personalized level, especially beneficial for patients and children previously excluded due to scan duration constraints. With the proposed consecutive prediction strategy, our model also sheds light on denoising and quality enhancement of other fMRI-related individualized studies.

Acknowledgments. This work was supported in part by NIH grants (MH116225, MH127544, MH123202, ES033518, AG075582, NS128534, and NS135574).

Disclosure of Interests. The authors have no competing interests to declare that are relevant to the content of this article.

References

1. Kong, R., Yang, Q., Gordon, E., Xue, A., Yan, X., Orban, C., Zuo, X.N., Spreng, N., Ge, T., Holmes, A. and Eickhoff, S.: Individual-specific areal-level parcellations improve functional connectivity prediction of behavior. Cerebral Cortex, 31(10), 4477-4500 (2021)
2. Wang, D., Buckner, R.L., Fox, M.D., Holt, D.J., Holmes, A.J., Stoecklein, S., Langs, G., Pan, R., Qian, T., Li, K. and Baker, J.T.: Parcellating cortical functional networks in individuals. Nature Neuroscience, 18(12), 1853-1860 (2015)
3. Finn, E.S. and Todd Constable, R.: Individual variation in functional brain connectivity: implications for personalized approaches to psychiatric disease. Dialogues in Clinical Neuroscience, 18(3), 277-287 (2016)
4. Hua, L., Gao, F., Xia, X., Guo, Q., Zhao, Y., Huang, S. and Yuan, Z.: Individual-specific functional connectivity improves prediction of Alzheimer's disease's symptoms in elderly people regardless of APOE ε4 genotype. Communications Biology, 6(1), 581 (2023)
5. Lebois, L.A., Li, M., Baker, J.T., Wolff, J.D., Wang, D., Lambros, A.M., Grinspoon, E., Winternitz, S., Ren, J., Gönenç, A. and Gruber, S.A.: Large-scale functional brain network

architecture changes associated with trauma-related dissociation. American Journal of Psychiatry, 178(2), 165-173 (2021)
6. Zhao, Y., Dahmani, L., Li, M., Hu, Y., Ren, J., Lui, S., Wang, D., Kuang, W., Gong, Q. and Liu, H.: Individualized functional connectome identified replicable biomarkers for dysphoric symptoms in first-episode medication-naïve patients with major depressive disorder. Biological Psychiatry: Cognitive Neuroscience and Neuroimaging, 8(1), pp.42-51(2023)
7. Paulo, D.L. and Bick, S.K.: Advanced imaging in psychiatric neurosurgery: toward personalized treatment. Neuromodulation: Technology at the Neural Interface, 25(2), 195-201 (2022)
8. Gordon, E.M., Laumann, T.O., Gilmore, A.W., Newbold, D.J., Greene, D.J., Berg, J.J., Ortega, M., Hoyt-Drazen, C., Gratton, C., Sun, H. and Hampton, J.M.: Precision functional mapping of individual human brains. Neuron, 95(4), 791-807 (2017)
9. Noble, S., Scheinost, D. and Constable, R.T.: A decade of test-retest reliability of functional connectivity: A systematic review and meta-analysis. Neuroimage, 203, p.116157 (2019)
10. Teeuw, J., Pol, H.E.H., Boomsma, D.I. and Brouwer, R.M.: Reliability modelling of resting-state functional connectivity. Neuroimage, 231, p.117842 (2021)
11. Cho, J.W., Korchmaros, A., Vogelstein, J.T., Milham, M.P. and Xu, T.: Impact of concatenating fMRI data on reliability for functional connectomics. Neuroimage, 226, p.117549 (2021)
12. Kaiser R.H., Andrews-Hanna J.R., Wager T.D., Pizzagalli D.A.: Large-scale network dysfunction in major depressive disorder A meta-analysis of resting-state functional connectivity. JAMA Psychiatry. 72, 603–611 (2015)
13. Dong D., Wang Y., Chang X., Luo C., Yao D.: Dysfunction of large-scale brain networks in schizophrenia: A meta-analysis of resting-state functional connectivity. Schizophr. Bull. 44, 168–181 (2018).
14. Elliott, M.L., Knodt, A.R., Cooke, M., Kim, M.J., Melzer, T.R., Keenan, R., Ireland, D., Ramrakha, S., Poulton, R., Caspi, A. and Moffitt, T.E.: General functional connectivity: Shared features of resting-state and task fMRI drive reliable and heritable individual differences in functional brain networks. Neuroimage, 189, 516-532 (2019)
15. Mejia, A.F., Nebel, M.B., Shou, H., Crainiceanu, C.M., Pekar, J.J., Mostofsky, S., Caffo, B. and Lindquist, M.A.: Improving reliability of subject-level resting-state fMRI parcellation with shrinkage estimators. NeuroImage, 112,14-29 (2015)
16. Nikolaidis, A., Heinsfeld, A.S., Xu, T., Bellec, P., Vogelstein, J. and Milham, M.: Bagging improves reproducibility of functional parcellation of the human brain. Neuroimage, 214, p.116678 (2020)
17. Coifman, R.R. and Lafon, S.: Diffusion maps. Applied and Computational Harmonic Analysis, 21(1), 5-30 (2006)
18. Bethlehem, R.A., Paquola, C., Seidlitz, J., Ronan, L., Bernhardt, B., Tsvetanov, K.A. and Cam-CAN Consortium: Dispersion of functional gradients across the adult lifespan. Neuroimage, 117299 (2020)
19. Nenning, K.H., Xu, T., Schwartz, E., Arroyo, J., Woehrer, A., Franco, A.R., Vogelstein, J.T., Margulies, D.S., Liu, H., Smallwood, J. and Milham, M.P.: Joint embedding: A scalable alignment to compare individuals in a connectivity space. Neuroimage, 222, p.117232 (2020)
20. Zhao, F., Xia, S., Wu, Z., Duan, D., Wang, L., Lin, W., Gilmore, J.H., Shen, D. and Li, G.: Spherical U-Net on cortical surfaces: methods and applications. In Information Processing in Medical Imaging: 26th International Conference, IPMI 2019, 26, pp. 855-866. Springer. (2019)

21. Zhao, F., Wu, Z., Wang, L., Lin, W., Gilmore, J.H., Xia, S., Shen, D. and Li, G.: Spherical deformable u-net: Application to cortical surface parcellation and development prediction. IEEE Transactions on Medical Imaging, 40(4), pp.1217-1228 (2021)
22. Van Essen, D.C., Smith, S.M., Barch, D.M., Behrens, T.E., Yacoub, E., Ugurbil, K. and Wu-Minn HCP Consortium.: The WU-Minn human connectome project: an overview. Neuroimage, 80, 62-79 (2013)
23. Gordon, E.M., Laumann, T.O., Gilmore, A.W., Newbold, D.J., Greene, D.J., Berg, J.J., Ortega, M., Hoyt-Drazen, C., Gratton, C., Sun, H. and Hampton, J.M.: Precision functional mapping of individual human brains. Neuron, 95(4), 791-807 (2017)
24. Yeo, B.T., Krienen, F.M., Sepulcre, J., Sabuncu, M.R., Lashkari, D., Hollinshead, M., Roffman, J.L., Smoller, J.W., Zöllei, L., Polimeni, J.R. and Fischl, B.: The organization of the human cerebral cortex estimated by intrinsic functional connectivity. Journal of Neurophysiology, 6,1125-1165 (2011)
25. Sohn, K.: Improved deep metric learning with multi-class n-pair loss objective. In: Advances in Neural Information Processing Systems, 1857–1865 (2016)
26. Qiu, W., Ma, L., Jiang, T. and Zhang, Y.: Unrevealing reliable cortical parcellation of individual brains using resting-state functional magnetic resonance imaging and masked graph convolutions. Frontiers in Neuroscience, 16, p.838347 (2022)
27. Glasser, M. F., et al.: The minimal preprocessing pipelines for the Human Connectome Project. Neuroimage, 80, 105-124 (2013).
28. Preti, M.G., Bolton, T.A., Van De Ville, D.: The dynamic functional connectome: State-of-the-art and perspectives. Neuroimage, 160, 41–54 (2017)
29. Hu, D., Wang, F., Zhang, H., Wu, Z., Zhou, Z., Li, G., Wang, L., Lin, W., Li, G. and UNC/UMN Baby Connectome Project Consortium: Existence of functional connectome fingerprint during infancy and its stability over months. Journal of Neuroscience, 42(3), pp.377-389 (2022).
30. Benkarim, O.M., Sanroma, G., Piella, G., Rekik, I., Hahner, N., Eixarch, E., González Ballester, M.A., Shen, D. and Li, G.: Revealing regional associations of cortical folding alterations with in utero ventricular dilation using joint spectral embedding. In Medical Image Computing and Computer Assisted Intervention 2018, 2018, pp. 620-627. Springer International Publishing. (2018)